

# Transient Classifiers for Fink

## Benchmarks for LSST

B.M.O. Fraga<sup>1\*</sup>, C.R. Bom<sup>1,2</sup>, A. Santos<sup>1</sup>, E. Russeil<sup>3</sup>, M. Leoni<sup>4</sup>, J. Peloton<sup>4</sup>, E.E.O. Ishida<sup>3</sup>, A. Möller<sup>5</sup>,  
and S. Blondin<sup>6,7</sup>

<sup>1</sup> Centro Brasileiro de Pesquisas Físicas, Rua Dr. Xavier Sigaud 150, Rio de Janeiro, Brazil

<sup>2</sup> Centro Federal de Educação Tecnológica Celso Suckow da Fonseca, Rodovia Márcio Covas, lote J2, Itaguaí, Brazil

<sup>3</sup> Université Clermont-Auvergne, CNRS, LPCA, 63000, Clermont-Ferrand, France

<sup>4</sup> Université Paris-Saclay, CNRS/IN2P3, IJCLab, 15 rue Georges Clemenceau, 91405 Orsay, France

<sup>5</sup> Centre for Astrophysics and Supercomputing, Swinburne University of Technology, Mail Number H29, PO Box 218, 31122 Hawthorn, VIC, Australia

<sup>6</sup> Aix Marseille Univ, CNRS, CNES, LAM, Marseille, France

<sup>7</sup> European Southern Observatory, Karl-Schwarzschild-Straße 2, Garching, D-85748, Germany

### ABSTRACT

**Context.** The upcoming Legacy Survey of Space and Time (LSST) at the Vera C. Rubin Observatory is expected to detect a few million transients per night, which will generate a live alert stream during the entire 10 years of the survey. This will be distributed via community brokers whose task is to select subsets of the stream and direct them to scientific communities. Given the volume and complexity of data, machine learning (ML) algorithms will be paramount for this task.

**Aims.** We present the infrastructure tests and classification methods developed within the FINK broker in preparation for LSST. This work aims to provide detailed information regarding the underlying assumptions, and methods, behind each classifier. Thus enabling users to make informed follow-up decisions from FINK photometric classifications.

**Methods.** Using simulated data from the Extended LSST Astronomical Time-series Classification Challenge (ELAsTiCC), we showcase the performance of binary and multi-class ML classifiers available in FINK. These include tree-based classifiers coupled with tailored feature extraction strategies, as well as deep learning algorithms. Moreover, we introduce the CBPF Alert Transient Search (CATS), a deep learning architecture specifically designed for this task.

**Results.** Results show that FINK classifiers are able to handle the extra complexity which is expected from LSST data. CATS achieved 97% accuracy on a multi-class classification while our best performing binary classifier achieve 99% when classifying the Periodic class.

**Conclusions.** ELAsTiCC was an important milestone in preparing the FINK infrastructure to deal with LSST-like data. Our results demonstrate that FINK classifiers are well prepared for the arrival of the new stream, but this experience also highlight that transitioning from current infrastructures to Rubin will require significant adaptation of currently available tools. This was the first step in the right direction.

**Key words.** methods: data analysis – surveys – supernovae:general

## 1. Introduction

The advent of large scale sky surveys has forced astronomy to enter the era of big data, with current experiments already producing data sets which challenge traditional analysis techniques (Hilbe et al. 2014). In this context, machine learning (ML) methods are almost unavoidable (e.g., Bamford et al. 2009; Baron 2019; Bom et al. 2022). For time-domain astronomy, the ability to quickly process the data and obtain meaningful results has become critical due to current and upcoming projects such as the Zwicky Transient Facility (ZTF, Bellm et al. 2019) and the Vera C. Rubin Observatory Legacy Survey of Space and Time (LSST, Ivezić et al. 2019), respectively. Such projects employ a difference imaging analysis pipeline which stream to community brokers, in the form of alerts, every detection above a given signal to noise threshold.

Brokers are subsequently tasked with filtering and analysing the data in detail, selecting the most promising objects for different science cases and redirecting them to different research communities. FINK (Möller et al. 2021) is one of the official LSST brokers, selected to receive the raw alert stream from the beginning of LSST operations<sup>1</sup>, expected for 2025. In the meantime, brokers systems are operating, and being tested, with alerts from ZTF. FINK ingests and process the stream, making use of several different science modules which contain cross-matching capabilities, ML classifiers and user-specified filters (for details on FINK see Möller et al. 2021, and references therein).

The experience accumulated in the last few years in FINK with ZTF has been paramount for the design, development and fine tune of the broker services according to

<sup>1</sup> Also selected were ALERCE (Förster et al. 2021), AMPEL (Nordin et al. 2019), ANTARES (Matheson et al. 2021), Babamul, LASAIR (Smith et al. 2019) and Pitt-Google.

\* e-mail: bernardo@cbpf.br

the needs of difference scientific communities. Beyond the scientific results already reported (see e.g., Aivazyan et al. 2022; Kuhn et al. 2023; Carry et al. 2024; Karpov & Peloton 2022) this partnership has enabled the development of a series of tools specifically designed to deal with the alert stream (Leoni et al. 2022; Biswas et al. 2023a; Russeil et al. 2022; Allam et al. 2023; Le Montagner et al. 2023; Biswas et al. 2023b; Karpov & Peloton 2023; Moller & Main de Boissiere 2022). Nevertheless, given the volume and complexity of the expected data, restructuring algorithms to transition from ZTF to LSST is a non-trivial task.

The Extended LSST Astronomical Time-Series Classification Challenge<sup>2</sup> (ELAsTiCC, Knop & ELAsTiCC Team 2023), developed by the LSST Dark Energy Science Collaboration (DESC), was created to allow a concrete assessment of the performance of different stages of the communication pipeline. This includes simulating an alert stream to be received by brokers, the ingestion and analysis of the alerts using ML based classifications by the broker teams, as well as reporting back such scores to DESC. In this work we use the first version of the ELAsTiCC data set, streamed between September 2022 and January 2023<sup>2</sup>, to stress-test the performance of the entire FINK infrastructure in an LSST-like data scenario.

This paper is organised as follows: in Section 2 we present the dataset, its properties, and our chosen experiment design; Section 3 presents with more details how FINK works, showing the preparations for LSST; Section 4 presents the metrics we will use to evaluate the classifiers; Section 5 gives more details about the construction and training of ML models, while Section 6 presents an evaluation of these models on a blind test set. We show how some classifiers can be combined to improve standalone performances in Section 7, and Sections 8 and 9 are left for discussions and conclusions, respectively.

## 2. The ELAsTiCC dataset

The “Extended LSST Astronomical Time-series Classification Challenge” (ELAsTiCC; Knop & ELAsTiCC Team 2023) was designed to test brokers systems and classification algorithms when applied to a state of the art data set which mostly resembles LSST alerts. It emerged from the experiences accumulated during two previous challenges: the SuperNova Photometric Classification Challenge (SNPCC, Kessler et al. 2010) and the Photometric LSST Astronomical Time-series Classification Challenge<sup>3</sup> (PLAsTiCC, Hložek et al. 2023) and is lead by the LSST Dark Energy Science Collaboration (DESC). Its first objective was to test the brokers infrastructure capability of ingesting and processing a real-time alert stream. The second goal was to enable the evaluation of ML classification algorithms.

In the first instance of the challenge (hereafter ELAsTiCCv1), two different simulated datasets were provided: a static set of full light-curves (1 light curve per astrophysical source) was made available in 18 May 2022 and an alert stream corresponding to 3 years of LSST operations was streamed between September 2022 and January 2023. Both datasets were simulated using SuperNova ANALYSIS package (SNANA, Kessler et al. 2009) and contained 19

<sup>2</sup> [https://portal.nersc.gov/cfs/lsst/DESC\\_TD\\_PUBLIC/ELASTICC/](https://portal.nersc.gov/cfs/lsst/DESC_TD_PUBLIC/ELASTICC/)

<sup>3</sup> <https://www.kaggle.com/c/PLAsTiCC-2018>

classes divided into 5 broad categories<sup>4</sup> (SN-like, Periodic, Non-periodic, Long and Fast). Light-curves, comprising detections and forced photometry in the LSST broad-band filters  $\{u, g, r, i, z, Y\}$  were provided (for details on how the simulation was generated we refer to the project website<sup>2</sup>). In order to isolate the performance of our classifiers, avoid issues due to the data generating process and circumvent the need to transform full light curves into alerts, we chose to use here only the streamed data set<sup>5</sup>.

We selected the first year of ELAsTiCCv1 as training sample for all our algorithms (17 233 868 alerts labelled from 27 November 2023 to 27 November 2024 and corresponding to 1 676 431 distinct objects). The remaining two years were used as a test set to evaluate the performance of our classifiers (34 872 745 alerts corresponding to 2 865 642 distinct objects).

The class distributions for the alerts in our train and test sets are shown in Figures 1 (unique classes) and 2 (broad classes). We note that in our experiment design, the population distributions between classes are similar in both samples, with SN types Ia and II comprising almost half of the alerts, and the Fast class being the least represented one. Overall, the distributions for the unique and broad classes are extremely imbalanced, which could pose a problem for multi-class classifiers.

Each alert package included both, light curve data (`mjd`, `fluxcal`, `fluxcal_err`, band-pass filter: `filtername`) as well as object metadata, comprised of properties such as position, milky way extinction and estimated photometric redshift, among others. In Fig. 3 we show the distributions for two of these properties for the training and test set: the milky way extinction (`mwebv`, left) and photometric host galaxy redshift (`hostgal_zphot`, right). Approximately 81% of the objects in the training set have a photometric redshift available, while this number is 91% in the test set. Despite this small difference, the distributions are similar, with both photometric redshift distributions displaying a double peaked structure.

Fig 4 shows the distribution of number of detection points per alert with and without forced photometry (left), as well as the global number of detection points in each bandpass (right), for the training (top) and test (bottom) sets. It can be seen from the top left panel that the distribution of light curve sizes considering only the detections is strongly peaked around 10 detections, dropping heavily after that, with very few alerts having more than 100 measurements in the training set. In the test set, although the distribution also peaks around 10 detections, there is a considerable number of alerts with more than 100 points, even without including forced photometry. This is a direct consequence of our experiment design, where the maximum time span of a light curve in the training set was cut to 1 year. This decision can impact the generalisation ability of some classifiers, specially when considering astrophysical sources whose light curve is expected to last for extended time periods (such as active galactic nuclei or super-luminous supernovae).

<sup>4</sup> Full taxonomy can be found at <https://github.com/LSSTDESC/elasticc/blob/main/taxonomy/taxonomy.ipynb>

<sup>5</sup> A second version, ELAsTiCCv2, was released in mid-2023, with updates in photometric redshift model and cadence. The second version was not used in this work.

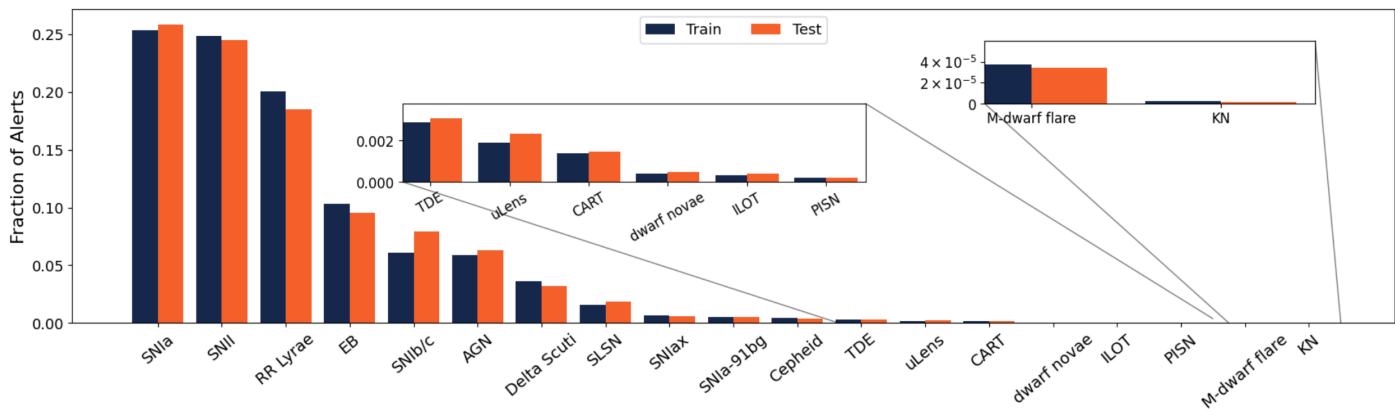


Fig. 1: ELAsTiCC class distribution for our training (dark blue) and test (orange) sets.

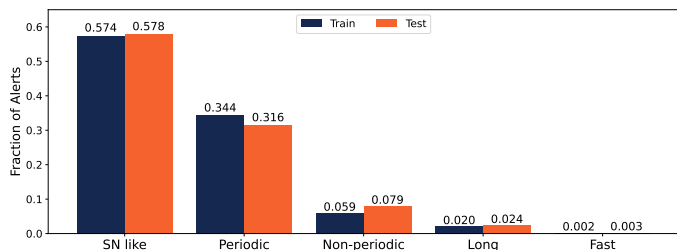


Fig. 2: ELAsTiCC broad class distribution for our training (dark blue) and test (orange) sets.

The distribution of detections per passband (right column of Figure 4) is similar for the training and test sets: the redder the band, the larger the maximum number of detections. The exception to this is the  $z$  band, which do not appear in longer lightcurves. This is especially important for classifiers that rely on colours or use only specific passbands. Nevertheless, this feature is a direct consequence of the chosen survey strategy, and it is reasonable to expect that the real data will also hold differences in number of detections on each band, thus it is paramount to access the robustness of classifiers in this scenario.

### 3. Fink Infrastructure

Since 2019, FINK has been processing alert data from the ZTF public stream. Not only the ZTF data rate is lower than the one intended for LSST, but the schema and content of the alert packets from each stream are also different. Therefore, the ELAsTiCC challenge was an opportunity to show that the Fink architecture can scale in terms of data volume and that it is possible adapt the current classifiers, or create new ones, to a new schema with different incoming information.

FINK operates in real time on large-scale computing infrastructures. For the ZTF processing, the incoming data stream is provided by the ZTF Alert Distribution System (ZADS, Patterson et al. 2018) that runs a Kafka instance on the DigitalOcean cloud infrastructure (USA). FINK is currently deployed on the VirtualData<sup>6</sup> cloud infrastructure (France), and makes use of distributed computing to split the incoming stream of alerts into smaller chunks of data

to be analysed independently over many machines in parallel. For LSST, FINK will be deployed at CC-IN2P3, which will have a local copy of LSST data that can be efficiently exploited for internal cross-match needs.

What is deployed for ZTF typical rates (of the order of 200,000 alerts per night) can be easily scaled to ELAsTiCC rates (of the order of 1,000,000 alerts in a few hours every night) by adding more machines. In practice for the challenge, we use a total of 33 cores for all operations (listening to the incoming stream, processing it and sending back results). Moreover, the processing was done on the same platform, alongside the real-time processing of ZTF alerts.

For the ELAsTiCC challenge, FINK operations consisted in three steps, done in real time: (1) decoding the incoming alert stream, (2) applying all classifiers on every alert, and (3) redistributing all enriched alert packets to the DESC team in the USA. The first and last steps are under the responsibility of the FINK engineering team, while the second part involves classifiers provided by the community of users. Each team responsible for a classifier typically provides a pre-trained model, as well as the snippet of code necessary to run the inference on one alert<sup>7</sup>, and the FINK engineering team integrates it into FINK for streaming processing at scale.

Given the large volume of data, we developed a new service for the community during the challenge, the FINK Data Transfer service<sup>8</sup>. The ELAsTiCC training set was made available via this service that enables easy distribution of large volumes of data for many decentralised users. This service allows users to select any observing nights, apply selection cuts based on alerts content, define the content of the output, and stream data directly anywhere. Since the start of the challenge, more than one billion alerts have been streamed via this service.

For the experiments described in this work, nine classifiers were deployed (see Sect. 5). Some of the classifiers used in the challenge are also classifiers used to process the ZTF alert stream. The differences in data rate, schema and the data itself (available filter bands, cadence and magnitude limit, among others) between the ZTF stream and

<sup>7</sup> The FINK engineer team provides examples to manipulate alert data, and all code and models can be found online at <https://github.com/astrolabsoftware/fink-science>.

<sup>8</sup> <https://fink-portal.org/download>

<sup>6</sup> <https://virtualdata.fr/>

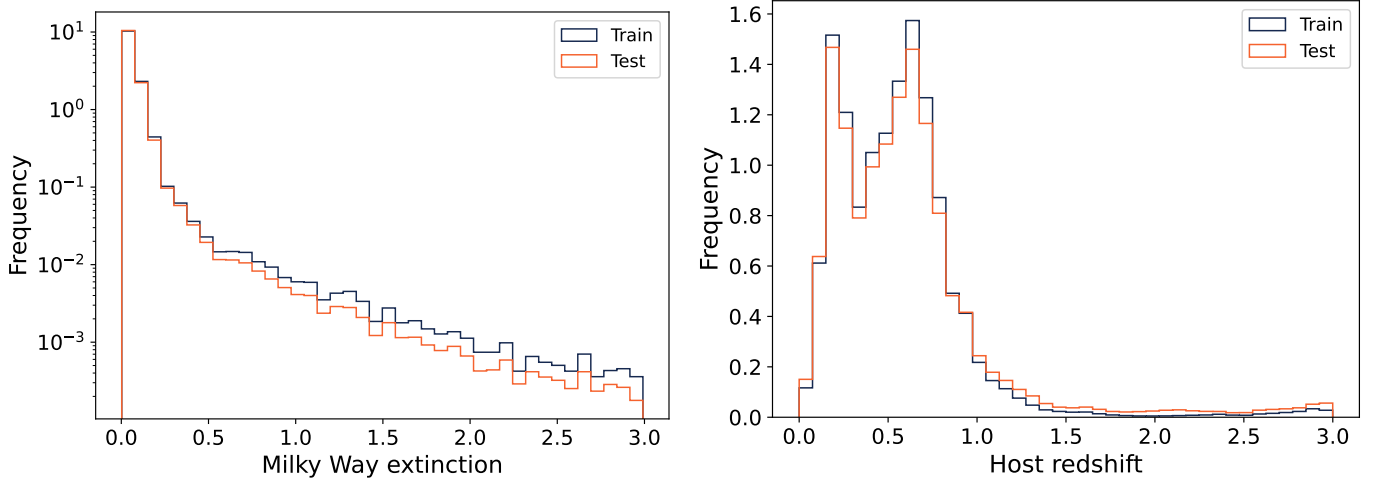


Fig. 3: Distribution of milky way extinction (left) and host galaxy photometric redshift (right) for the training (dark blue) and test (orange) sets.

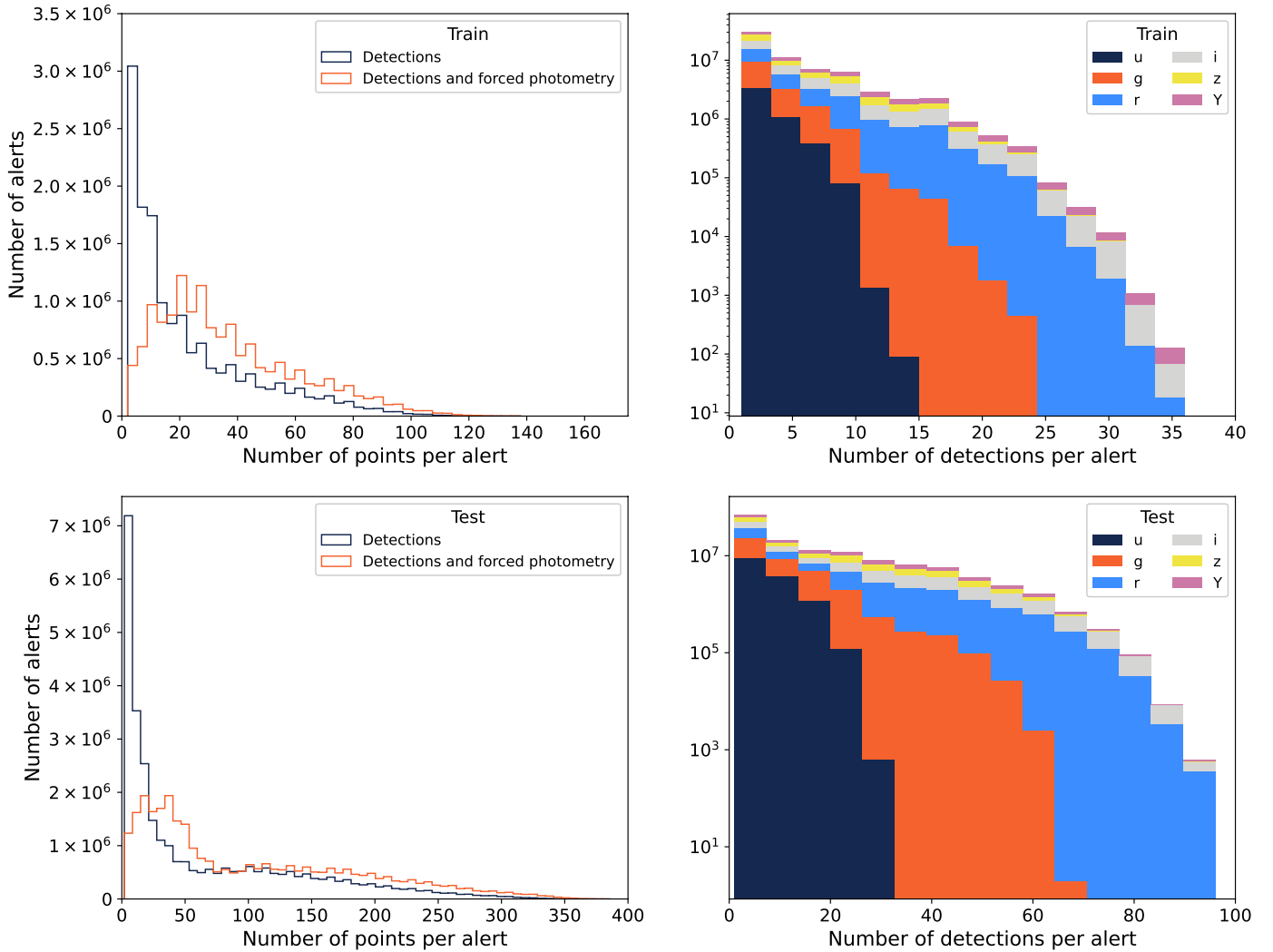


Fig. 4: Distribution of light curve length in the training (top) and test (bottom) samples. On the left, the total number of points including only detections (blue) and with forced photometry (orange). On the right, the distribution of detections per filter.

the simulated ELAsTiCC data made the transition less easy than we had originally anticipated. From this point of view, the lessons learned from the ELAsTiCC challenge were paramount in preparing for the arrival of the LSST alert stream.

Throughout the classifier design phase and the challenge itself, we monitor classifier performance in terms of throughput (alerts processed/second/core) and memory usage (MB/core). LSST will impose stringent requirements on throughput (we expect a continuous flow of 10,000 alerts per exposure, i.e. every 30 seconds), while our computing infrastructure imposes constraints on memory usage (cores with 2 GB RAM each). As an example, while processing in real-time the first version of the challenge (using 24 cores in parallel), 82.2% of alerts were classified in less than 30 seconds (the time between when an alert enters FINK and when it is fully classified by the nine classifiers), 90.5% in less than a minute, and over 99.9% in less than 10 minutes. Delays larger than expected are partly due to processing (classifier versions and performance have evolved over time), but the high values are mainly explained by human intervention in the computing infrastructure, which interrupted operations while we were processing live data. These interventions are not expected during normal LSST operations. Regular measurements of Fink operations performance (profiling) are analyzed to check that requirements are met.

#### 4. Metrics

In a classification task, several metrics can be used to assess the performance of the classifier, such as the Receiver Operating Characteristic (ROC) and Precision-Recall curves, and the Confusion Matrix. These are built from the Precision (P), Recall (R, also called the True Positive Rate, TPR) and False Positive Rate (FPR), which in a binary classification are defined as

$$\begin{aligned} P &= \frac{TP}{TP + FP}, \\ R &= \frac{TP}{TP + FN}, \\ FPR &= \frac{FP}{FP + TN}, \end{aligned} \quad (1)$$

with TP(N) the number of true positives (negatives) and FP(N) the number of false positives (negatives). Precision can be understood as the purity of the predictions, while Recall is its completeness or efficiency, and the FPR is the ratio of wrongly classified objects of the negative class (also known as the false alarm rate). The output of a binary classifier is a the probability of a light curve belonging to the class of interest. Thus, the quantities on Eq. 1 will depend on a chosen probability threshold. By varying this threshold, one can obtain curves for Recall vs FPR (ROC) and Precision vs Recall. The area under these curves (AUC) can be used as a metric to assess the performance of the classifier, where a perfect classifier would have an AUC of 1 and an AUC of 0.5 for the ROC corresponds to a random classifier.

The binary case can be straightforwardly extended to the multi-class case by using a *one vs all* approach, wherein the problem is split into a binary classification case per class, gathering every class except one as the negative class.

In this case, there will be a ROC and a Precision-Recall curve for every single class.

Another popular metric for classification task is the Confusion Matrix, a square matrix showing the number (or percentage) of objects classified in every combination true/predicted class. Both metrics will be used to access the efficiency of classifiers described in this work.

## 5. Classifiers in Fink

### 5.1. CATS

Recurrent Neural Networks (RNNs) are a class of models adapted to work with sequential data. They do so by constructing hidden states that carry information from the previous part of the sequence (Rumelhart & McClelland 1987; Schmidt 2019). One of the main problems found in training RNNs was the vanishing gradients: when the input sequence was long, the successive derivatives during backpropagation tended to erase the gradient (Bengio et al. 1994), which then cause later timesteps to be “disconnected” from earlier ones (i.e., a low memory capacity). Long-Short Term Memory units (LSTM, Hochreiter & Schmidhuber 1997) were designed to avoid the vanishing gradient problem by keeping not only a hidden state, but also a memory state across all timesteps. By using gates, the network can learn what information needs to be kept, removed, or inserted to the memory vector, increasing the RNN’s memory capacity.

The CBPF Alert Transient Search (CATS) was built by starting with a base network very similar to the Multivariate LSTM Fully Convolutional Network (MLSTM-FCN, Karim et al. 2019), using squeeze and excitation blocks; we use bidirectional LSTM layers and a series of fully connected layers before the output, adding a dropout layer after each of those. This architecture was shown to perform very well in several different time series tasks<sup>9</sup>, and the base architecture is shown in Fig 5 We then perform a hyperparameter search using keras-tuner, searching for the best configuration of number of convolutional, LSTM and Dense blocks, convolutional filters, LSTM and Dense layers’ units and activation functions. This search was done using a subset of 10% of the unique objects in our training sample to speed up the process. The final architecture consists of one convolutional block with 32 filters, two bidirectional LSTM layers with 400 and 500 units respectively, and two fully connected layers with 64 and 96 units. All convolutional and fully connected layers are followed by a Rectified Linear Unit (ReLU) activation.

Our inputs are the normalised flux and errors, (where both are normalised per light curve), and the gap in days to the first alert, using forced photometry when available. To that, the filter is added as an integer in the range [1, 6] corresponding to the LSST passbands, [u, g, r, i, z, Y]. All inputs were right-padded to match the longest light curve, so that the shape of the input is (140, 4) (top-right box in Fig. 5). To this, we concatenated the Milky Way extinction (mwebv), host galaxy redshift (hostgal\_zphot), and the redshift of the transient (z\_final), when available, plus their errors (Input metadata) before passing the result to the fully connected layers. Using these features gave the

<sup>9</sup> See <https://paperswithcode.com/task/time-series-classification> for benchmarks on several different time series tasks.

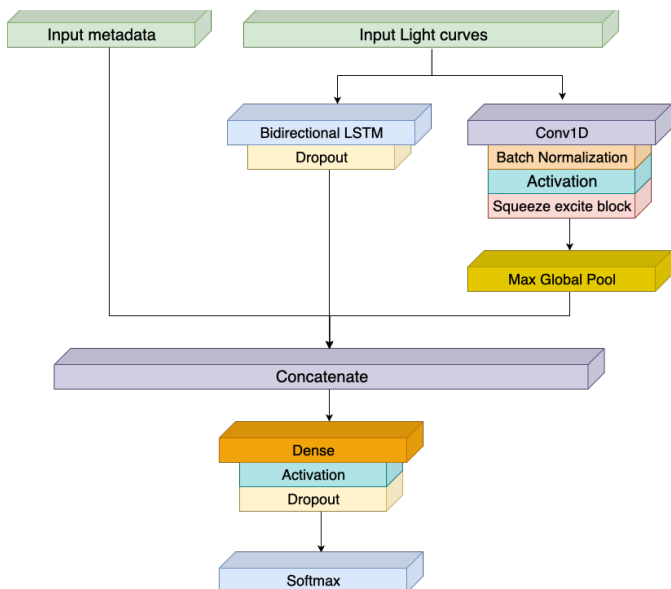


Fig. 5: Illustration of the CATS architecture.

best results when testing with a smaller subset of the data, slightly better than using only extinction and redshift of the host.

We perform a  $K$ -fold cross-validation process to assess the robustness of our model. It consists of splitting the data into  $k$  groups (folds), and performing  $k$  iterations of training; at each iteration, one of the folds is used for testing, while the other  $k - 1$  are used for training.

We used five folds, and a subset consisting of 80% of the unique objects in the training set to perform our cross-validation. The unique object identifier (`diaObjectId`) was the parameter used to split the data, thus making every light curve of a single object either part of the training or validation set, with no contamination between them.

The model was trained for 12 epochs at each fold, with the Rectified Adam optimizer (Liu et al. 2020), on a cluster with eight NVIDIA RTX 3090. At each fold, the model where the validation loss was lowest was selected to perform the predictions. The architecture and training were implemented using TensorFlow 2 (Abadi et al. 2015).

Table 1 shows the metrics derived from the validation sets of the  $k$ -fold. The model performed satisfactorily, having a mean ROC AUC above 0.95 for all classes, and a mean Precision-Recall AUC above 0.8 except for the Long class, with little variance between the folds. Although the mean Precision for the Long class is nearly 80%, the Recall is less than 50%, due to half of the Long alerts being classified as SN-like events. The major type behind this confusion are SLSN, which could resemble some types of supernovae when looking at short enough light curves. On the other hand, the 20% rate of false positives of the Long class is dominated by SNII, which is also the dominant subclass, with SNIa a close second; however, SNIa contamination is negligible. These results are a direct consequence of our choice of training sample. The maximum duration of a light curve in the training sample is one year, which understandably renders SLSNe very similar to other SN types, specially SNII with an extended plateau phase. SNIa at low and medium redshift are in general brighter than other SN types and exhibit a characteristic feature in redder passbands, thus rendering

their classification less controversial. Despite such caveats, results shown in Table 1 confirm that CATS will be able to provide reliable classification results even under challenging data scenarios.

	ROC AUC	PR AUC	Precision	Recall
SN-like	0.99 (0.0002)	0.99 (0.0003)	0.97 (0.002)	0.99 (0.001)
Fast	0.99 (0.0009)	0.82 (0.017)	0.89 (0.012)	0.71 (0.03)
Long	0.96 (0.0025)	0.65 (0.014)	0.79 (0.031)	0.47 (0.03)
Periodic	1.00 (0.00001)	1.00 (0.00003)	1.00 (0.0002)	1.00 (0.0001)
Non- Periodic	1.00 (0.00003)	1.00 (0.0005)	0.97 (0.003)	0.96 (0.005)

Table 1: Mean results for the validation sample across all folds, with standard deviations in parentheses. ROC AUC and PR AUC are the area under the curve for the ROC and Precision-Recall curves, respectively, while the values for the Precision and Recall are taken from the confusion matrix averaged over all folds.

## 5.2. SuperNNova (SNN)

SUPERNNova (SNN; Möller & de Boissière 2019) is a deep learning light-curve classification framework based on Recurrent Neural Networks. SUPERNNova makes use of fluxes over different band-passes and their measurement uncertainties over time for classification of time-domain candidates in different classes. Additional information such as host-galaxy redshifts and Milky Way extinction and their errors can be included to improve performance.

SNN includes different classification algorithms, such as LSTM Recurrent Neural Networks and two approximations for Bayesian Neural Networks (BNNs). Here, we only use the LSTM architecture, which was also used for classification of type Ia SNe (SNe Ia) in the Dark Energy Survey (Möller et al. 2022, 2024). For work on BNNs in the context of Rubin see Moller & Main de Boissiere (2022).

We use the LSTM RNN to process the photometric time series and produce a sequence of hidden states. The sequence is condensed to fixed length through mean pooling. Finally, a linear projection layer is applied to obtain an  $N$ -dimensional vector, where  $N$  is the number of classes. A softmax function is used to obtain probabilities for an input to belong to a given class. During training, we randomly truncate light-curves to improve the robustness of the classifier with partial light-curves. SNN is trained to optimize accuracy of balanced classes.

We grouped observations in each passband within a given night. If a given filter is not observed, we assigned it a special value to indicate that it is missing. To deal with irregular time sampling, we added a delta time feature to indicate how much has elapsed since the last observation. We used the default configuration of SNN with the normalisation as in (Möller et al. 2022) and added redshift and Milky Way extinction as additional features for this work.

Classification probabilities from SNN can be used to select a sample by performing a threshold cut or by weighting the contribution of candidates by their classification score

Class	Accuracy	ROC AUC	Precision	Recall
SN-like	97.18	0.9937	95.68	97.70
Fast	99.04	0.9976	99.52	98.57
Long	83.79	0.9198	89.04	77.64
Periodic	99.59	0.9999	99.48	99.76
Non-Periodic	99.59	0.9999	99.48	99.76
Broad	87.96	-	77.61	67.53

Table 2: SUPERNNova performance for complete light-curves using an independent test set from the first year of alerts. All rows except the last one show the metrics for a binary target vs. other types.

(Vincenzi et al. 2023, 2024; DES Collaboration 2024). In this work we evaluate only the selection of samples using a probability cut set to  $p > 0.5$  or in multi-class classification, the largest probability for all classes.

We train binary and broad class models. For the binary classification, we balance the training set light-curve numbers between the target class and other classes (randomly sampled). For the broad classifier we do also a balanced training set. However, the Fast, Long and Non-periodic classes have considerably smaller numbers than the SN and Periodic classes as shown in Figure 2; the balanced training set for broad classification is  $\approx 2,000$  events per class.

We split the dataset in 80% for training, 10% for validation and 10% for performance evaluation. In Table 2, we show the performance metrics for the different models obtained for this test set.

For the broad model, we find that the most misclassified classes are SNe and Long events. This may be due to the time-range of the light-curve provided for classification as some Long events such as PISN and SLSNe during a reduced time range may resemble shorter time-scale SNe. We also find small confusion between Fast and Periodic transients that may be due to the same effect.

For the binary models, we also find that the model targeting Long events has lower accuracies than the other binary classification models. This may be due to the small dataset used for training which is composed of only thousands of light-curves.

As expected, small and unbalanced training sets impact the performance of this framework which was built for accurate classification with large and representative training sets. Further discussion on the performance of SUPERNNova with respect to training set size can be found in Möller & de Boissière (2019).

### 5.3. Superluminous Supernovae

Superluminous supernovae (SLSN) are SNe whose peak optical luminosity exceeds  $-21$  mag (see, e.g., Moriya et al. 2018 for a review). Their rise times can vary between  $\sim 20$  days to more than 100 days for some events, but their post-maximum decline rates are either consistent with  $^{56}\text{Co}$  decay (at least initially), or significantly faster. This suggests that some SLSN can have a possible thermonuclear origin, which given the mass required can only be explain by population III star origin. At such mass, a pair production mechanism triggers and results in an instability which eventually leads to the collapse of the core, hence, pair-

instability SNe (PISN). Currently, there have been no direct confirmation of their existence, although good candidates have been reported (Moriya et al. 2022; Pruzhinskaya et al. 2022). The discovery and characterisation of a PISN would significantly impact our understanding of the connection between chemical evolution and structure formation in the Universe (LSST Science Collaboration et al. 2009).

Given that predicted light curves of SLSN and PISNe can have a similar morphology, we use a common classifier for both and call it the SLSN classifier. Its core implementation is based on a feature extraction of normalised alerts followed by a random forest classification. For each filter we compute the following set of features: maximum and standard deviation of the flux; mean signal to noise ratio and number of points. We also added the following metadata information: right ascension (`ra`), declination (`dec`), host galaxy photometric redshift (`hostgal_zphot`), host galaxy photometric redshift error (`hostgal_zphoterr`) and distance between the host and the transient (`hostgal_snsep`). In addition, parametric fits of the light curves in passbands  $r$  and  $i$  are computed using the following 3-parameter function:

$$f(t) = A(t - t_0) \times e^{-\frac{t-t_0}{t_{fall}}}, \quad (2)$$

which depends on amplitude ( $A$ ), a time offset ( $t_0$ ) and a characteristic time of decay ( $t_{fall}$ ). We found this simple functional form to be effective in classifying both SLSN-I and PISN, although it cannot match precursor emission or fluctuations in the light curve. This equation was obtained by applying the Multi-View Symbolic Regression algorithm (Russeau et al. 2024) to real ZTF light curves from the SLSN candidate SNAD160<sup>10</sup> (Pruzhinskaya et al. 2022). An example of a SLSN fit is shown in Figure 6. The minimisation was performed using the SCIPY library (Virtanen et al. 2020) with a RMSE loss. The optimised parameters and the RMSE loss are included as features for the classifier, thus we impose that, for each alert, light curves in passbands  $r$  and  $i$  contain at least 3 observed points. Finally, standard deviation and maximum absolute value of the  $r - i$  colour were calculated.

The colour estimation for this data is non-trivial. Due to the irregular sampling, simultaneous pair of points in different filters almost never exist. We use the interpolation previously computed from Equation 2 to estimate the colour. The observed points in a band were used in combination with the estimated light curve in the other band so the colour could be computed. In total, 39 features are extracted for each alert.

The classifier was based on a scikit-learn random forest algorithm trained using the active learning (AL) procedure proposed in Leoni et al. (2022). This strategy allows the classifier to focus on the relevant boundaries between SLSN and similar transients rather than simply learning the global distribution between very unbalanced classes. This procedure tends to favour purity over completeness, which is reasonable given the volume of alerts that will be produced by LSST. To proceed we randomly sample 3 million alerts, from the first year of ELAsTiCCv1, which were equally divided in training and validation samples. We query 6 alerts at a time for 3500 loops (further queries resulted in overfitting - thus performance decrease) for a final

<sup>10</sup> <https://ztf.snad.space/dr17/view/821207100004043>

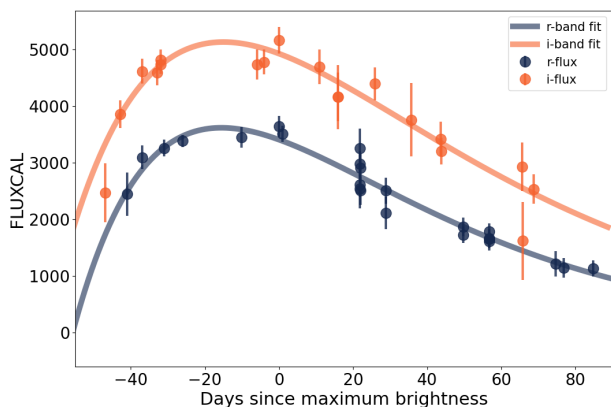


Fig. 6: Best fit on  $r$  and  $i$  passbands of a SLSN (`alertId` = 231155714092) using Equation 2. The fits are used to compute colour evolution (Section 5.3). Parameters of the fit as well as least square errors are kept as features. Optimised parameters for  $r$  and  $i$  passbands are respectively  $A = 245$ ,  $t_0 = 55.7$ ,  $t_{fall} = -40.0$  and  $A = 291$ ,  $t_0 = 62.9$ ,  $t_{fall} = -47.6$ .

training sample composed of 21100 alerts. We set the maximum depth of trees and minimum number of alerts per leaf are set to be 15 and 0.01 % of the training size, respectively. The model achieved 84.6 % purity and 44.4 % completeness in the classification of SLSN from the validation sample.

#### 5.4. Early Supernova Ia

Supernovae Ia (SNIa) were first used as standard candles in cosmological analysis in the end of the 20<sup>th</sup> century, when they provided the first evidence of the Universe’s current accelerated expansion (Riess et al. 1998; Perlmutter et al. 1999). Since then, large efforts have been devoted to the compilation of large SNIa samples, in the hope they can help unravel details about the behaviour of dark energy (e.g., Aleo et al. 2023; Möller et al. 2024).

Despite the undeniable impact large scale sky surveys can imprint on SN cosmology results, such potential is strongly dependent on our ability to distinguish SNIa from other types of SN-candidates (see e.g., Ishida 2019, and references therein). In the context of real data, labelling is an extremely expensive process and ideally we would like to discover such transients early enough so they are still sufficiently bright to allow spectroscopic classification.

For ZTF processing, FINK has an early supernova Ia classifier (hereafter, EarlySNIa) based on independent feature extraction for each of the 2 ZTF passbands and a random forest classifier enhanced by active learning (for a complete description see Leoni et al. 2022). The module has been successfully reporting EarlySNIa candidates to TNS since November/2020. However, in the context of LSST, with 3 times more passbands and a considerable sparser cadence, the module required significant modifications.

In order to allow classification with a lower number of points per filter and, at the same time, take into account color information, we implemented the RAINBOW multi-band feature extraction method proposed by Russeil, E. et al. (2024) to comply with the characteristics of the new data set. A parametric model was simultaneously fitted to the light-curves in all available passbands, and the best-

fit parameter values were used as features, thus given as input to the random forest classifier (Ho 1995). Assuming the transient can be approximated by a black-body, the framework combines temperature and bolometric light curve models to construct a 2-dimensional continuous surface. This approach enables early description even when the number of observations in each filter is significantly limited (for more details see Russeil, E. et al. 2024).

The preprocessing for each alert included: i) averaging all observations within the same night; ii) removing any intra-night flux measurements lower than -10 ( $\text{FLUXCAL} > -10$ ); iii) requiring a minimum of 7 points per object, in any filter, including forced photometry and iv) ensuring that intra-night flux measurements are consistently increasing within at least 2 passbands. Thus, considering that only rising alerts survived such selection cuts, we described the bolometric evolution of our light-curves with a logistic function of the form:

$$f(t) = \frac{\text{amplitude}}{1 + \exp\left(-\frac{t-t_0}{\text{rise\_time}}\right)} \quad (3)$$

where `rise_time` is the characteristic time of rise, `amplitude` is the amplitude and  $t_0$  describes a reference time which corresponds to the time at half of the rising light curve. The temperature evolution was described with a falling logistic function of the form:

$$T(t) = T_{\min} + \frac{\text{delta\_T}}{1 + \exp\left(\frac{t-t_0}{\text{k\_sig}}\right)}, \quad (4)$$

where `delta_T` is the full amplitude of temperature,  $T_{\min}$  denotes the minimum temperature reached, `k_sig` describes a characteristic timescale and  $t_0$  is a reference time parameter which corresponds to the time at half of the slope. Note that  $t_0$  from the bolometric and temperature descriptions are used as a single common parameter whose role is to anchor functional behaviour but which holds no physical meaning without a reference point, thus it was not included in our final parameter set. Beyond these, RAINBOW also returns a measurement of the quality of the fit (`reduced_chi2`) and the maximum measured flux (`1c_max`). Figure 7 illustrates the capability of the method in extrapolating the behaviour of a rising light curve even when the number of rising points is sparse. In this figure, the model (full lines) was fit using only the history within the alert (circles). The most recent observation (cross) was added subsequently as a way to compare the measurement with the prediction.

As a result, each alert is represented by 7 values. To this we added the mean signal to noise ratio ( $\text{FLUXCAL}/\text{FLUXCALERR}$ ); the number of points in all passbands before intra-night smoothing<sup>11</sup> (`nobs`); separation between the host and the transient (`hostgal_snsep`) and the host photometric redshift (`host_photoz`). Thus resulting in 11 parameters per alert.

A total of 6 457 832 alerts (998 594 objects) survived selection cuts, which correspond to  $\approx 37\%$  of the entire training sample. Among them, SNIa ( $\approx 31\%$ ), SNIId ( $\approx 25\%$ ), RR Lyrae ( $\approx 17\%$ ) and Ibc ( $\approx 7\%$ ) were the most frequent

<sup>11</sup> This number was obtained by counting the number of observations and each alert, not the corresponding metadata column.



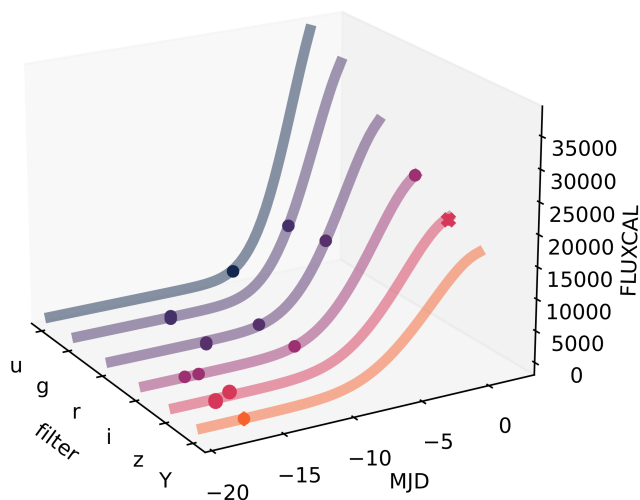


Fig. 7: Example of light curve fit for an early SNIa performed with RAINBOW. The estimated light curve behaviour in each filter (full lines) was found by using the photometric history within `alertId = 244687224069` (circles). The most recent observation within that alert (cross) was added subsequently to illustrate the agreement between the estimation and measured value in the  $z$ -band.

classes. From these we selected a sample of 114 701 alerts (60 489 objects) for designing our experiments. In this sample, the distribution of the major classes was unchanged, but the representation of smaller classes was inflated to allow training the ML model. For example, we ensured that the least represented class (KN) comprised  $\approx 1\%$  of the sample used for training. Note that we report populations of individual classes to better illustrate the composition of the sample, but in summary, we trained a binary classifier whose positive class corresponded to approximately a third of the full sample. We used half of the unique object identifiers (`diaObjectId`) for training and the other half for validation to avoid information leak between the two subsets.

We trained a random forest model using a scikit-learn (Pedregosa et al. 2011) implementation, using 50 trees, maximum depth of 15 and set the minimum number of alerts per leaf to be 0.01 % of the training size. In the surviving training sample, this resulted in  $P = 0.69/R = 0.66$ , considering a probability threshold of 0.5.

## 6. Classifiers Performance

In this Section we evaluate the different classifiers available in FINK using the test sample composed of the two final years of ELAsTiCCv1. In Section 7 we show how combining different classifiers can boost classification results.

Figure 8 shows the ROC (left) and Precision-Recall (center) curves and the confusion matrix (right) for each classifier; each cell in the confusion matrix displays the precision (on top, bold) and the recall (bottom, italics). Besides these overall metrics, we analyse in Figure 9 how metrics change with: the number of detections and the true host redshift (ZHELIO from the truth table). This allows us to assess the ability of classifiers to generate unbiased samples,

and their capabilities as a tool to select follow-up sources close to the time of detection.

### 6.1. CATS Broad Classification

Figure 8a shows the metrics for the CATS broad classifier. Similar to the cross-validation results presented in Section 5.1, the model performs excellently with the SN-like, Periodic and Non-Periodic classes, having AUCs above 0.95 for all of them. However, again similar to the earlier results, it had problems with the Long class: more than half of the alerts were classified as SN-like, which is a result of the choice of training set. On the other hand, the precision improved, reaching  $\sim 87\%$ , compared to  $\sim 79\%$  for the training set.

The Fast class is where the results differ the most between the first and the last two years of simulations. The AUC of Precision-Recall curve dropped to 0.63 compared to 0.82 in first year, driven by a decrease in the number of Fast alerts correctly classified by our model. More than half of the Fast alerts were classified as Periodic, the same confusion the model had in the training set albeit to a smaller degree. A possible reason for this behaviour is the different distribution of number of detections for the two sets. Most correctly classified alerts of the Fast class in the training set have between 20 and 180 points. Since the training set is capped at one year, they form the majority of the total number of alerts, making the recall larger. On the test set, however, CATS incorrectly classified every alert with more than 200 points (there are very few light curves this size in the first year). Since it spans two years, a sizeable number of alerts have more than 200 points, contributing to a lower recall than in the training set. Due to this decrease in recall, the precision increased to above 90%, making CATS a useful tool to generate pure transient samples of every class. If we restrict the test set to only alerts with 150 points or less, the results are very similar to the training set, showing that the main contributing issue to the difference in performance is the difference in light curve length.

In Figure 9a, it can be seen that CATS is able to correctly classify samples with less than 10 detections, obtaining a precision of over 80% for every class, and nearly 100% for SN-like events. However, above  $\sim 120$  detections, the precision for SN-like alerts decrease as the number of detections grow, due to SLSN alerts being classified as SN-like. This is understandable since one of the defining characteristics of SLSNe light curves is a longer decay time, which can make long SN look like SLSN especially when brightness is not a factor, since the light curves were normalised. Recall for the SN-like class behaves similarly, but the decrease only happens after  $\sim 150$  detections, the model misclassifies SN-like alerts as non-periodic. A similar trend is seen for the Fast class, but now the confusion is with Periodic alerts.

When looking at the metrics as a function of redshift, the precision for SN-like alerts drop as the simulated redshift increases: this is due to SLSN alerts being classified as SN-like. The opposite is seen for the Long class, where low redshift alerts are classified as SN-like.

## 6.2. SUPERNNNOVA as a Broad Classifier

We show the performance metrics and confusion matrix in Figure 8b for SNN broad classifier. As found when validating the model, both the SN and Long classes have large classification confusion. In Figure 9b we see this confusion is reduced with more detections as the classifier disentangles Long and SNe light-curves with more precision.

As with the CATS classifier, the Fast class is where the results differ the most between the first and the last two years of simulations with a similar trend of confusion between Fast and Periodic light-curves.

We highlight, that the loss used to train SUPERNNNOVA is optimised for classification with large and representative training sets. In Möller & de Boissière (2019), we have shown that  $\approx 10^5$  light-curves per class for training are necessary to achieve its top performance. To improve performance with ELASTICC, the loss could be modified to allow the usage of non-balanced training sets and/or larger training sets could be constructed with additional simulations or augmentation techniques. We leave this task for future work.

## 6.3. SUPERNNNOVA binary classifiers

We find better performance for the SN-like classification with the binary classifier (Figure 8c) than with the broad one. This suggests, as expected, that the increase of the training set for the target is extremely important for our algorithm. We also find an improvement for classes with smaller training sets such as Fast (Figure 8d) and Long (Figure 8e). However, these two classes still are challenging to classify.

The evolution of metrics as a function of number of detections and redshift for the SNN binary classifiers are shown in Figures 9c, 9d, 9e, 9f, 9g. The same trend as in the broad classifier is found, our Long classifier increases its precision as more detections are available (Figure 9e). Non-Periodic classification (Figure 9f) is found to be very stable with respect of number of detections and redshift provided. Periodic and SN-like classification also show stable performance with respect to number of detections (Figure 9g). Thus, we expect a good performance in the classification of early light-curves for these classes. This is an important feature when scheduling follow-up observations as explored for Rubin SNe Ia in Möller et al. (2024).

We highlight, that the binary classifiers presented in this work were all trained in a similar manner without tuning SNN to the different targets. Depending on the science goal, data curation, loss and algorithm hyper-parameters could be adjusted to improve its performance. For example, to improve Fast transients classification we could train with shorter light-curves for all classes, an augmented training set or a modified loss to tackle small training sets. As shown in Möller et al. (2022) for SNe Ia, an adequate light-curve time-span selection for a given goal to reduce non-transient detections improves performance.

## 6.4. Superluminous Supernovae

Figure 8h displays the ROC curve of the binary SLSN classifier. It provides an excellent purity of 91.2 % with a relatively low recall of 27.4 %. In the context of the very large ELASTICC data set, we favour this high precision low recall

asymmetry as it would still result in more than 100K SLSN alerts being classified with high confidence in the validation sample. Compared to the testing sample, we observe a 6.6% improvement of precision and a 17% decrease in completeness. This variation in behaviour is explained by the long scale evolution of some SLSN, which may last more than a year. Given that the training sample considered only the first year of ELASTICCv1 the model has not been trained to identify the longest SLSN. This is illustrated in Figure 9h where the peak of recall reaches up to 50% between 50 and 150 detections, but largely drops with further detections where SLSN are missed. On the other hand, we observe that the precision linearly increases with the number of detections. Finally the classifier presents a clear under performance in precision and recall for objects with redshift lower than 0.5. Indeed SLSN are intrinsically bright objects which are more frequently found at high redshift (corresponding large observation volumes), therefore a large majority of the sample has redshift above 0.5 (with a maximum around  $z=1$ ). It results in a challenging learning task at low redshift, which impacts the final performances. Outside of this range, the classifier is conservative and therefore very reliable on positive answers.

## 6.5. Early SNe Ia

The performance of the EarlySNIa classifier is reported in Figure 8i. One caveat we should keep in mind is that the module is only interested in classifying rising light curves. Thus, several alerts are eliminated by selection cuts, never being classified at all. Results presented here correspond to alerts that survived the feature selection (Section 5.4). Among these, the module was able to achieve  $\sim 0.7$  precision and recall. Meaning the the precision was maintained while recall increased slightly when compared to results from the validation sample. The most common contaminants are: SN II ( $\sim 18\%$ ) and SNIbc ( $\sim 9\%$ ). All other classes correspond to the remaining 3%, with SNIa-91bg and SNIax comprising  $\sim 1\%$  each.

Figure 9i shows how classification results evolve with the number of detections and simulated redshift. We note that precision already starts higher than 0.6 for 7 observed data points (the minimum requirement) and peaks around 20 photometric points, while recall remains almost stable even with more detections. The sample identified as EarlySNIa by the algorithm is highly skewed towards small light curves, with  $\sim 75\%$  of them having 10 detections or less. Moreover, since we are working only with rising behaviours, it is reasonable to expect that light curves with lower number of points will dominate the results. In this figure, we can also observe that classification results peak for redshift around 0.5 and degrades after that. This is expected, since the SN is most likely to be discovered at or after maximum when at high redshifts.

## 7. Combining classifiers

Given the wealth of developed classifiers targeting different science cases, combining some of them could provide better results. In this session we investigate the effectiveness of considering ensembles of two classifiers built from intrinsically different algorithms in order to boost classification results.

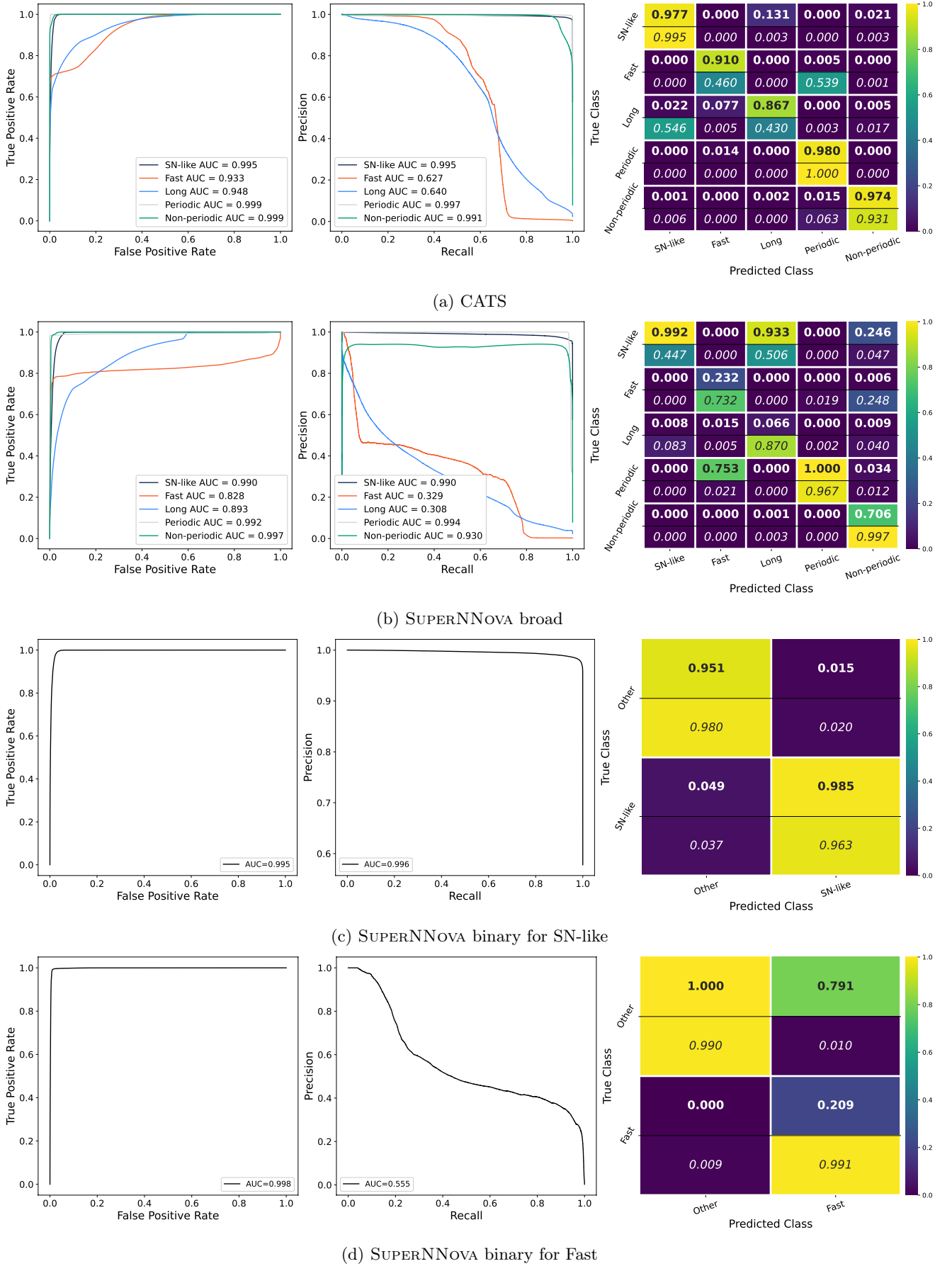
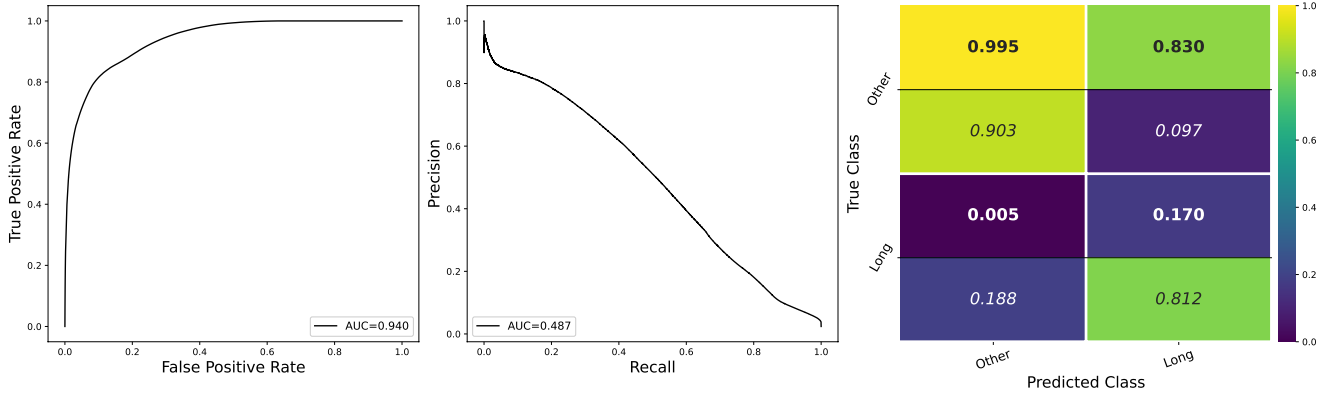
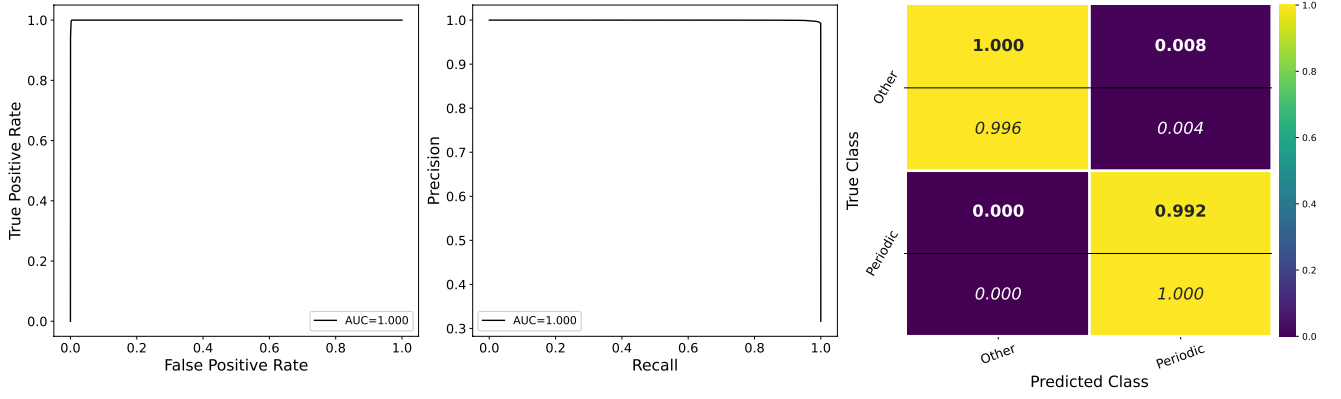


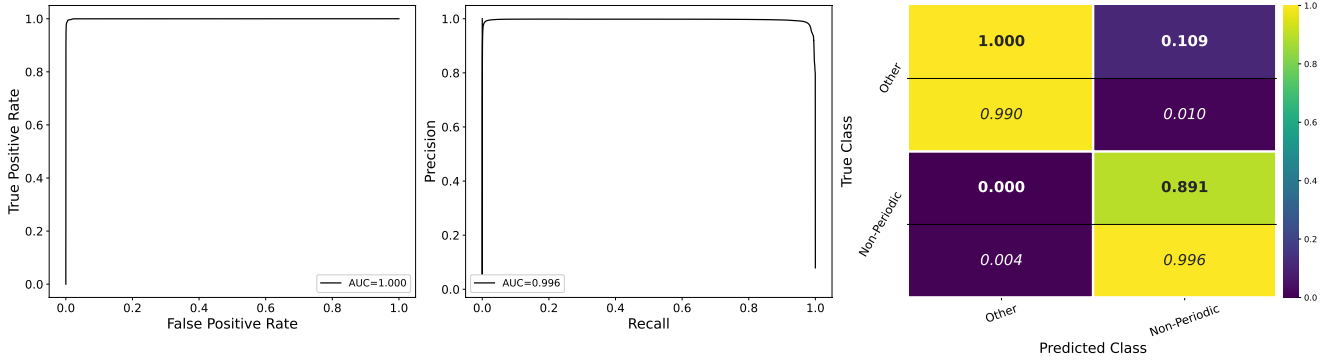
Fig. 8: ROC (left) and Precision-Recall (center) curves, and confusion matrix (right) for the classifiers in the test set. For each cell in the confusion matrix, precision is shown on top in bold, and recall at the bottom in italics.



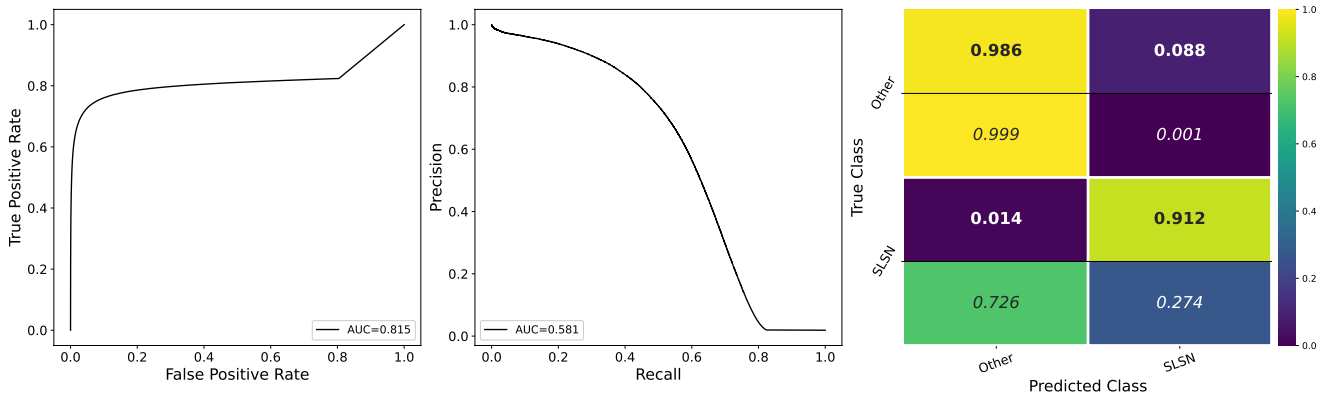
(e) SUPERNNova binary for Long



(f) SUPERNNova binary for Periodic



(g) SUPERNNova binary for non-Periodic



(h) SLSN

Fig. 8: Continued.

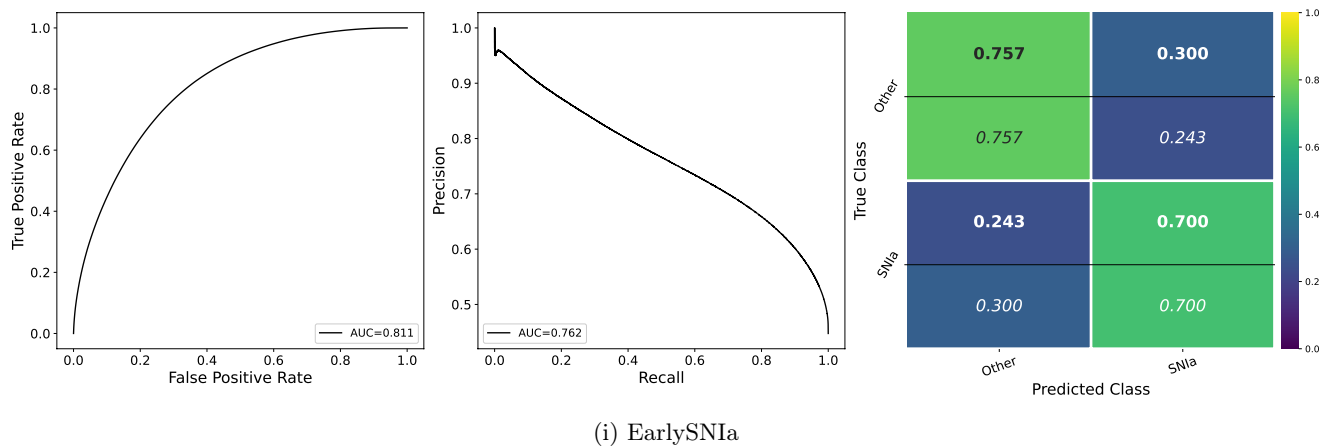


Fig. 8: Continued.

### 7.1. Broad classifier as a first step

We investigate the possibility of building a hierarchical classifier, where a broad classifier is initially applied to remove a large part of the contaminants, passing its results to a binary, more specific, model, possibly resulting in a more pure sample. We explore here using CATS before the SLSN classifier. Since the EarlySNIa binary classifier has the majority of contaminants within the SN-like broad class, so a previous broad classifier is not expected to impact their results.

We take only the alerts that CATS classified as Long to assess the performance of the SLSN classifier. Results are shown in Fig. 10, where we can see improvement in both, precision (from 0.912 to 0.966) and recall (0.274 to 0.470), together with both AUCs (from 0.815/0.581 to 0.869/0.946 values for ROC/PR). Albeit small, this improvement could help producing more reliable follow-up catalogues with very few contaminants. The fraction of false negatives increased, simply due to the sample to be classified by the SLSN binary classifier being smaller.

The total completeness from this sample is approximately 22%, a small decrease when compared to the binary classifier alone. This comes mainly from missing SLSNe, while the fraction of misclassified PISNe lowers by approximately 8%; an important result since PISNe are one of the least represented objects in the test set.

### 7.2. SUPERNNNOVA binary into a broad classifier

Given that SNN has one binary classifier for each broad class, we can combine them to create a multi-class classifier, potentially outperforming the broad SUPERNNNOVA model. In order to obtain ROC and Precision-Recall curves, we join together all probabilities for all five binary broad classifiers and apply a softmax function to the probability vector, similar to what a standard DL multi-class classifier does. The predicted class is considered to be the one with highest probability. We note that there are a few light curves (approximately 0.5%) that have all binary probabilities less than 0.5, i.e., the models did not classify it as any of the broad classes. These alerts are mainly from the SN-like class, with SNIa the majority. We nevertheless assign the broad class with the highest probability to them, since it will not impact the results.

Results are presented in Fig. 11 where we see a considerable improvement over the broad SUPERNNNOVA classifier. Since SUPERNNNOVA requires balanced samples for training, the limitation on the number of alerts is applied on each class separately, instead of all classes being limited by the least represented. The model now is presented with more variety during training, and the probability of the correct class are improved.

### 7.3. Combining classifiers for purity

Given the large volume of data LSST is expected to deliver on a daily basis, being able to build extremely pure samples out of tens of millions of light curves is extremely important, especially for follow-up purposes. Some of the models presented in Section 5 target the same class (or broad class); therefore, one way to improve the purity is to combine classifiers by only considering alerts that have been assigned the same class when presented to intrinsically different classifiers.

We analyse how our broad classification may be improved using CATS and the SUPERNNNOVA binary classifiers combined, which agree on the predicted class for  $\sim 94\%$  of the alerts. We show the confusion matrix over this sample in Fig. 12, where it can be seen that the results have improved so that all classes in this subsample now have precision above 0.9. The most challenging classes to identify, Fast and Long, almost double their precision with a small reduction on their recall.

## 8. Discussion

Our results show that all classifiers had mostly satisfactory performance for their classes of interest, with very few exceptions. Despite the difference in models and training methods in the classifiers, a few common trends emerged.

All broad classifiers had trouble identifying the Fast and Long classes, both for the validation and test sets; CATS and SUPERNNNOVA (both the broad and the combined binary classifiers) had different issues, with the former having higher purity and the latter higher completeness. Furthermore, looking at Figs. 8a and 11, both CATS and SUPERNNNOVA combined mixed up the same classes: Long and SN-like, Fast and Periodic. This suggests that the similarity of the classes is intrinsic to the dataset. On the other hand, the

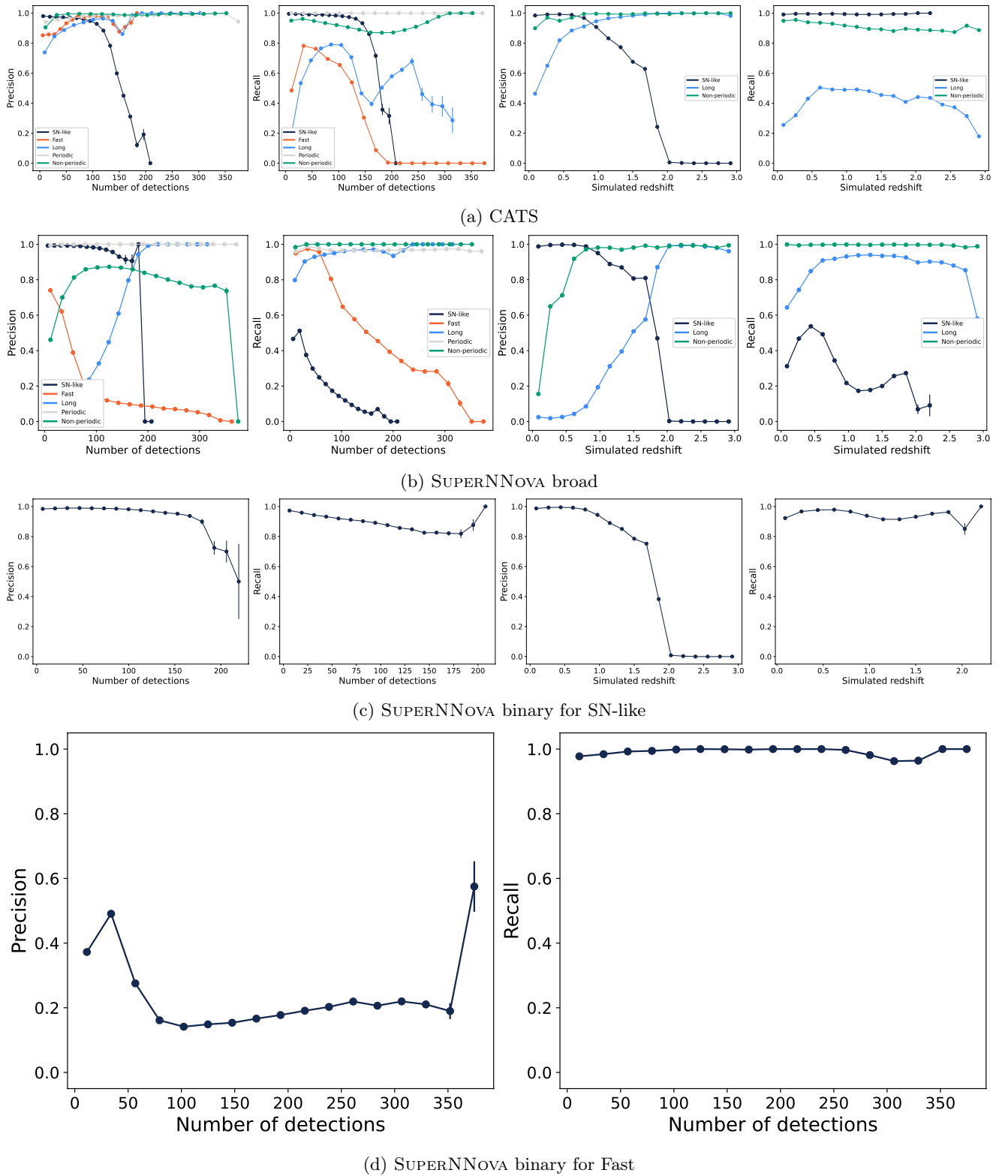


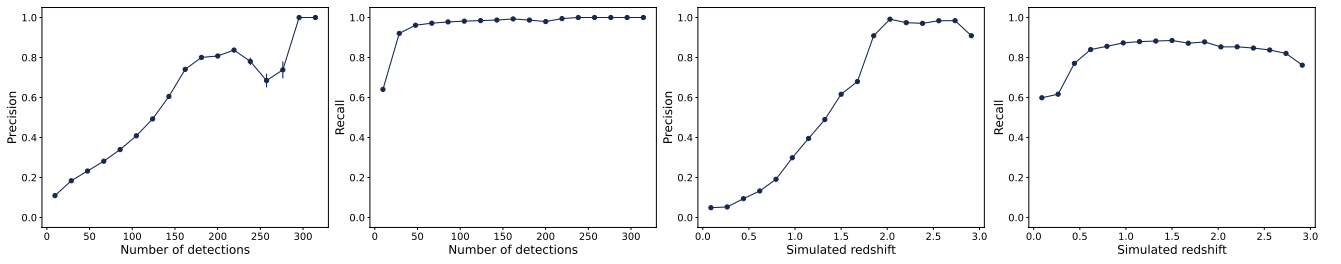
Fig. 9: Evolution of Precision and Recall as a function of number of detections (left two panels) and host galaxy redshift (right two panels). Fast and Periodic alerts have no redshift available and thus have only the first two panels.

difficulty to classify both the Long and Fast broad classes could be due to the one-year cap of the training data, since they are time-sensitive classes.

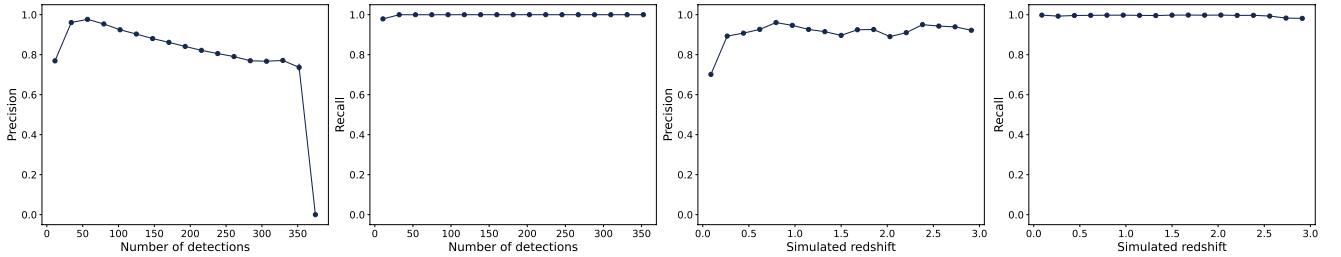
The Periodic broad class is very well characterised in the data, with all multi-class classifiers achieving almost perfect purity and completeness. Indeed, the light curves

for variable stars show a very distinctive periodicity, making them easy to identify among the other classes.

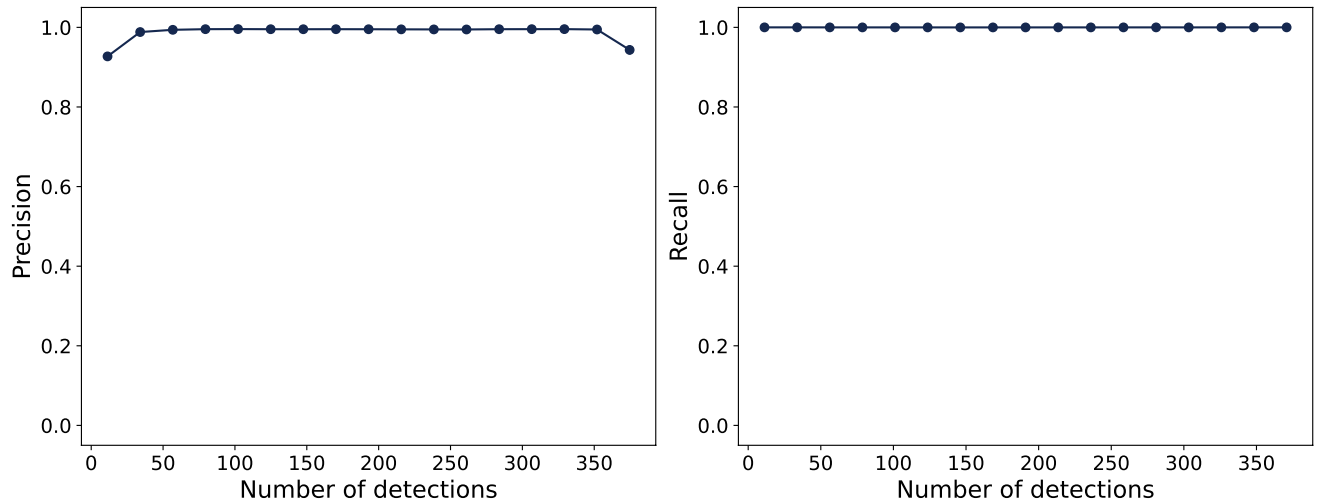
CATS can be used as a first step in a hierarchical classification scheme, in which it sends to binary classifiers only the alerts belonging to their respective broad class. When applied to the SLSN classifier, it showed a small increase in



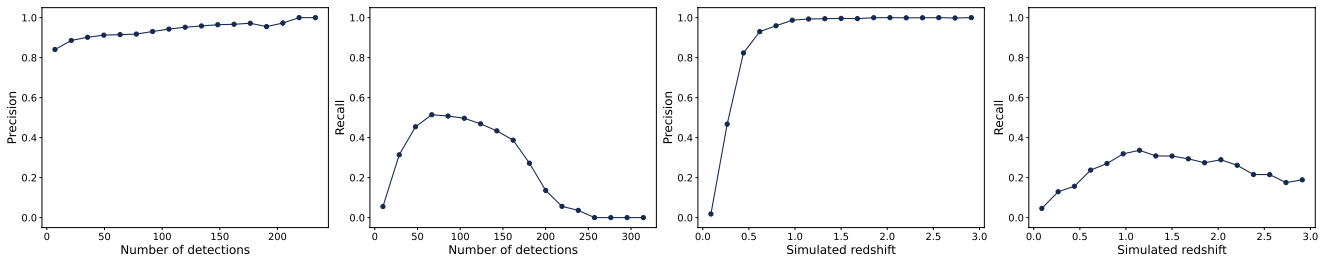
(e) SUPERNNOVA binary for Long



(f) SUPERNNOVA binary for non-Periodic



(g) SUPERNNOVA binary for Periodic



(h) SLSN classifier

Fig. 9: Continued

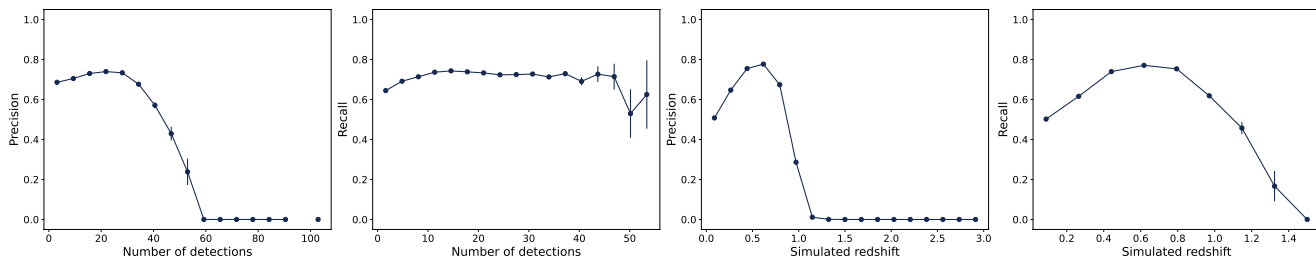
purity, even though both classifiers were not meant to work together in the first place. The in-sample completeness almost doubles compared to SLSN by itself.

The false positives of the EarlySNIa classifier are all within the SN-like broad class. This in turn means that using a broad classifier as a first step will not help improve its results.

SUPERNNOVA binary classifiers have better performance than the broad classifier for most classes. Given the current configuration of SNN, binary classifiers leverage

better small training sets. Additionally, binary classifiers can be tuned to the target goal and improve performance with simple actions such as light-curve length selection and hyper-parameter variation.

SUPERNNOVA binary classifiers can be combined into one multi-class model, with better performance than its broad classifier. SNN is lightweight and thus it is feasible to do this without impacting LSST processing. A similar approach could be used by other broad classifiers, although care must be taken that the model is lightweight enough so



(i) EarlySNIa

Fig. 9: Continued

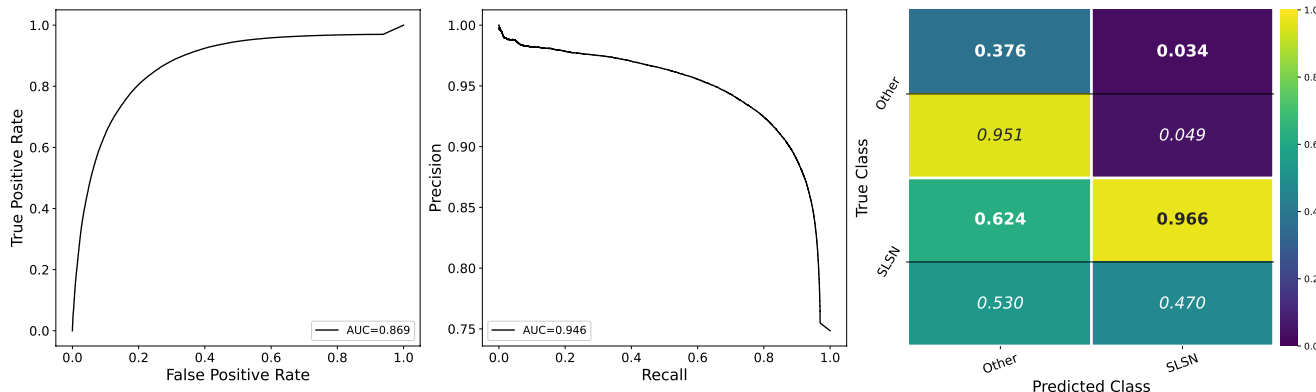


Fig. 10: Performance metrics for the SLSN classifier applied to the sample of alerts classified as Long by CATS.

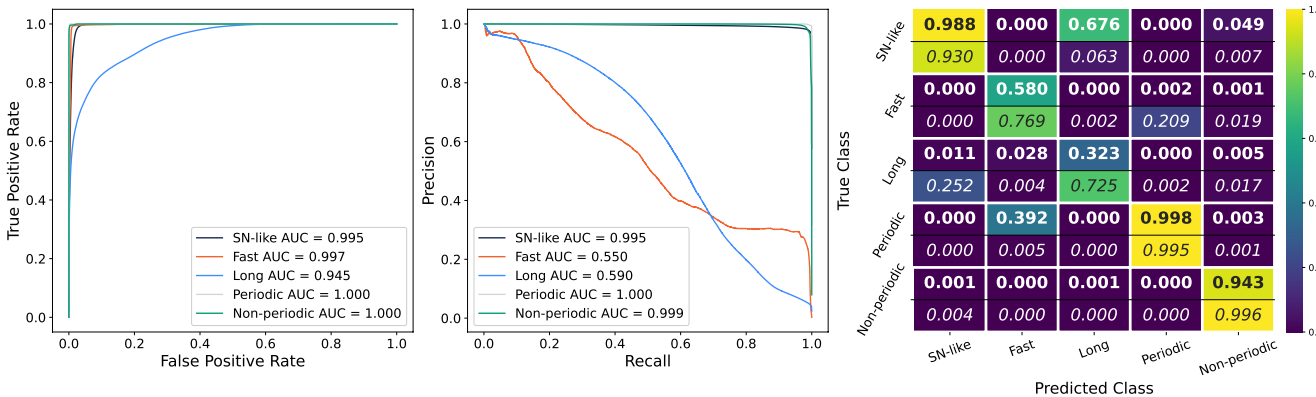


Fig. 11: Performance metrics for the combined SUPERNNNOVA binary classifiers.

that the extra computational cost does not affect the time necessary to process the alerts.

Samples with close to perfect purity can be built by requiring two or more classifiers to match their predictions. Combining CATS and all SUPERNNNOVA binaries improves significantly the results for the Fast and Long classes, the most difficult ones to classify.

### 9. Conclusions

For a few years now, broker teams have been successfully working with the ZTF alert stream and communication protocols as a test bench for what is to be expected for LSST. This experience has been extremely successful and has allowed the development of an entire broker ecosystem, along with a diverse and interdisciplinary community who sup-

ports it. Nevertheless, as valuable as this experience has been, it is also crucial to prepare our infrastructure for the important, and challenging, differences between the data delivered by these two experiments.

ELAsTiCC is a kind reminder that, beyond hardware and data format, machine learning models and broker infrastructure will need to change significantly in order to fulfil expectations which rise with the arrival of LSST. This includes the design of algorithms themselves, protocols for massive data transfer between geographically disconnected science teams, experiment design for proper evaluation and optimisation of trained models to allow processing of millions of alerts per night. The analysis presented here describes the strategies developed by the FINK team to address these issues.



We introduced CATS, a Deep Learning classifier built especially to work with LSST data for broad classification, which has shown great performance. Other classifiers, including SUPERNNova and tree-based models, were adapted from their current use on ZTF data. The adapted models performed well in their respective classification tasks, delivering pure and/or complete subsamples. Moreover, we also show examples of how different algorithms can be used to build an ensemble classifier which outperforms results from individual algorithms.

Nevertheless, it is important to keep in mind that FINK operates in a framework where each classifier (science module) is developed independently by different science teams. Processing is centralised by the FINK infrastructure but model development is geographically and scientifically distributed. This means that each team has a different scientific goal in mind when developing their own classifier.

Given 9 different classifiers (plus the combined ones) working at different tasks and showing different strong points, it is paramount to clarify the requirements for each science case so the user can make an informative decision when applying the models presented here. CATS for example, can produce pure samples for every class, but the combined SUPERNNova binaries have a better completeness for the Fast and Long classes. In the future, it will be important to tailor models and/or combine different ones to achieve top performance for a given science goal.

We also call attention for details which should be kept in mind when interpreting the classification results stated here. The choice of a training sample is of utmost importance in ML problems regarding both, their sample sizes and representativity. Compared to its predecessor PLAsTiCC, the objective of the ELAsTiCC challenge was the classification of alerts, i.e. partial views of complete light curves. Faced with the two different possibilities for training set, we chose the streamed alerts since they most resemble the test set and results are more easily transferable to

what is expected from LSST. In addition, the split between training and a blind test set was a practical one. In the future, different experiment designs may be attempted to avoid the inherent biases that arise from cutting the data in time.

Moreover, it is crucial to recognise that training a machine learning model implies access to the data and to the necessary hardware to process it. During this challenge, a new service was designed by FINK so that each team could access the curated data necessary for the training. This service was able to serve millions of alerts regularly to various teams, where the training of the models was largely performed on commodity hardware. Despite the undoubtedly usefulness of the data transfer service, irrespective of the volume of data to be transferred, we note that at the LSST scale, training models will require user teams to access dedicated hardware accelerators hosted on large data centres. This is an area where FINK is actively planning on providing, thus enabling a service for the community to train models at scale.

Considering the practical observational application of the classification results, early identification is paramount for the optimisation of follow-up resources and a major task of alert brokers. We have shown that most of our ML algorithms are capable of obtaining high-precision classification with less than 20 points. As more observations are added, the models generally give more accurate results. For the SN-like and Fast classes this performance increase is only valid with detection time-spans related to their variability.

In summary, we have shown that FINK is able to process ELAsTiCC alerts in a fast and efficient manner, as well as provide informative ML classification scores for a variety of science cases. This proves the adequateness of the FINK infrastructure and ML algorithms to process the big data volumes of Rubin LSST and, consequently, contribute to the realisation of its scientific potential.

## Acknowledgements

We thank Robert Knop, Gautham Narayan, Rick Kessler and all others involved in the development of ELAsTiCC for enabling this work. We thank Konstantin Malanchev for adapting the `light_curve` feature extraction package<sup>12</sup> (Malanchev et al. 2021) for use within the EarlySNIa classifier. This work was developed within the FINK community and made use of the FINK community broker resources. FINK is supported by LSST-France and CNRS/IN2P3. This is a result from the 2022 Fink Hackathon, 19 - 26 November 2022, Grimentz, Switzerland. This work received funding from CNRS MITI Evènements Rares - 2022, under project number 226696, Finding the first generation of stars with LSST (Fink). AM is supported by the ARC Discovery Early Career Researcher Award (DECRA) project number DE230100055. This work was supported by the ‘Programme National de Physique Stellaire’ (PNPS) of CNRS/INSU co-funded by CEA and CNES. CRB acknowledges the financial support from CNPq (316072/2021-4) and from FAPERJ (grants 201.456/2022 and 210.330/2022) and the FINEP contract 01.22.0505.00 (ref. 1891/22). BMOF, CRB and AS acknowledge the LITCOMP/COTEC/CBPF multi-GPU development team for all the support in the artificial in-

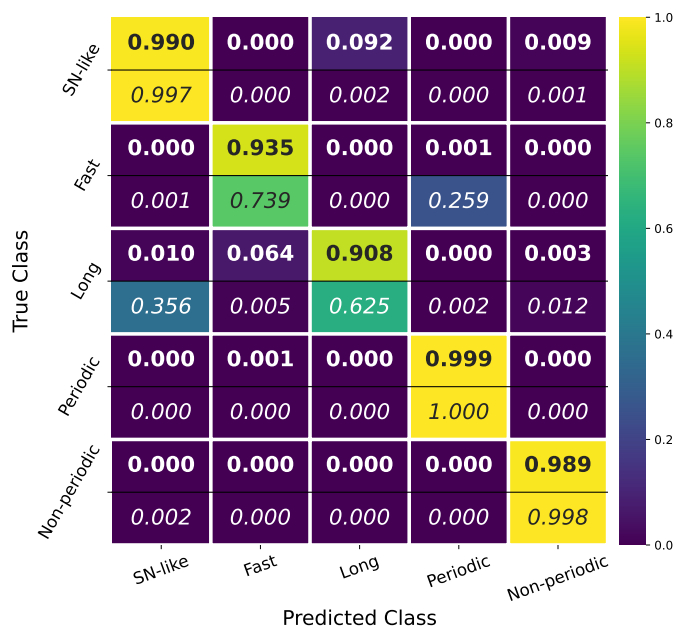


Fig. 12: Confusion Matrix for the alerts where CATS and the combined SUPERNNova binary agree.

<sup>12</sup> <https://github.com/light-curve/light-curve-python>

telligence infrastructure and Sci-Mind's High-Performance multi-GPU system.

## References

- Abadi, M., Agarwal, A., Barham, P., et al. 2015, TensorFlow: Large-Scale Machine Learning on Heterogeneous Systems, software available from tensorflow.org
- Aivazyan, V., Almualla, M., Antier, S., et al. 2022, MNRAS, 515, 6007
- Aleo, P. D., Malanchev, K., Sharief, S., et al. 2023, ApJS, 266, 9
- Allam, Tarek, J., Peloton, J., & McEwen, J. D. 2023, arXiv e-prints, arXiv:2303.08951
- Bamford, S. P., Nichol, R. C., Baldry, I. K., et al. 2009, MNRAS, 393, 1324
- Baron, D. 2019, arXiv e-prints, arXiv:1904.07248
- Bellm, E. C., Kulkarni, S. R., Graham, M. J., et al. 2019, PASP, 131, 018002
- Bengio, Y., Simard, P., & Frasconi, P. 1994, IEEE Transactions on Neural Networks, 5, 157
- Biswas, B., Ishida, E. E. O., Peloton, J., et al. 2023a, A&A, 677, A77
- Biswas, B., Lao, J., Aubourg, E., et al. 2023b, arXiv e-prints, arXiv:2311.04845
- Bom, C. R., Fraga, B. M. O., Dias, L. O., et al. 2022, MNRAS, 515, 5121
- Carry, B., Peloton, J., Le Montagner, R., Mahlke, M., & Berthier, J. 2024, arXiv e-prints, arXiv:2403.20179
- DES Collaboration. 2024, arXiv e-prints, arXiv:2401.02929
- Förster, F., Cabrera-Vives, G., Castillo-Navarrete, E., et al. 2021, AJ, 161, 242
- Hilbe, J. M., Riggs, J., Wandelt, B. D., et al. 2014, Significance, 11, 48
- Hložek, R., Malz, A. I., Ponder, K. A., et al. 2023, ApJS, 267, 25
- Ho, T. K. 1995, in Proceedings of 3rd international conference on document analysis and recognition, Vol. 1, IEEE, 278–282
- Hochreiter, S. & Schmidhuber, J. 1997, Neural Computation, 9, 1735
- Ishida, E. E. O. 2019, Nature Astronomy, 3, 680
- Ivezić, Ž., Kahn, S. M., Tyson, J. A., et al. 2019, ApJ, 873, 111
- Karim, F., Majumdar, S., Darabi, H., & Harford, S. 2019, Neural Networks, 116, 237
- Karpov, S. & Peloton, J. 2022, arXiv e-prints, arXiv:2202.05719
- Karpov, S. & Peloton, J. 2023, Contributions of the Astronomical Observatory Skalnaté Pleso, 53, 69
- Kessler, R., Bassett, B., Belov, P., et al. 2010, PASP, 122, 1415
- Kessler, R., Bernstein, J. P., Cinabro, D., et al. 2009, PASP, 121, 1028
- Knop, R. & ELAsTiCC Team. 2023, in American Astronomical Society Meeting Abstracts, Vol. 55, American Astronomical Society Meeting Abstracts, 117.02
- Kuhn, M. A., Benjamin, R. A., Ishida, E. E. O., et al. 2023, Research Notes of the American Astronomical Society, 7, 57
- Le Montagner, R., Peloton, J., Carry, B., et al. 2023, A&A, 680, A17
- Leoni, M., Ishida, E. E. O., Peloton, J., & Möller, A. 2022, A&A, 663, A13
- Liu, L., Jiang, H., He, P., et al. 2020, in International Conference on Learning Representations
- LSST Science Collaboration, Abell, P. A., Allison, J., et al. 2009, arXiv e-prints, arXiv:0912.0201
- Malanchev, K. L., Pruzhinskaya, M. V., Korolev, V. S., et al. 2021, MNRAS, 502, 5147
- Matheson, T., Stubens, C., Wolf, N., et al. 2021, AJ, 161, 107
- Möller, A. & de Boissière, T. 2019, MNRAS, 491, 4277
- Moller, A. & Main de Boissiere, T. 2022, in Machine Learning for Astrophysics, 21
- Möller, A., Peloton, J., Ishida, E. E. O., et al. 2021, MNRAS, 501, 3272
- Möller, A., Smith, M., Sako, M., et al. 2022, MNRAS, 514, 5159
- Möller, A., Wiseman, P., Smith, M., et al. 2024, arXiv e-prints, arXiv:2402.18690
- Moriya, T. J., Inserra, C., Tanaka, M., et al. 2022, Astronomy & Astrophysics, 666, A157
- Moriya, T. J., Sorokina, E. I., & Chevalier, R. A. 2018, Space Sci. Rev., 214, 59
- Nordin, J., Brinnel, V., van Santen, J., et al. 2019, A&A, 631, A147
- Patterson, M. T., Bellm, E. C., Rusholme, B., et al. 2018, Publications of the Astronomical Society of the Pacific, 131, 018001
- Pedregosa, F., Varoquaux, G., Gramfort, A., et al. 2011, Journal of Machine Learning Research, 12, 2825
- Perlmutter, S., Aldering, G., Goldhaber, G., et al. 1999, ApJ, 517, 565
- Pruzhinskaya, M., Volnova, A., Kornilov, M., et al. 2022, Research Notes of the American Astronomical Society, 6, 122
- Riess, A. G., Filippenko, A. V., Challis, P., et al. 1998, AJ, 116, 1009
- Rumelhart, D. E. & McClelland, J. L. 1987, Learning Internal Representations by Error Propagation, 318–362
- Russeau, E., Ishida, E. E. O., Le Montagner, R., Peloton, J., & Moller, A. 2022, arXiv e-prints, arXiv:2211.10987
- Russeau, E., Olivetti de França, F., Malanchev, K., et al. 2024, arXiv e-prints, arXiv:2402.04298
- Russeau, E., Malanchev, K. L., Aleo, P. D., et al. 2024, A&A, 683, A251
- Schmidt, R. M. 2019, arXiv e-prints, arXiv:1912.05911
- Smith, K. W., Williams, R. D., Young, D. R., et al. 2019, Research Notes of the AAS, 3, 26
- Vincenzi, M., Brout, D., Armstrong, P., et al. 2024, arXiv e-prints, arXiv:2401.02945
- Vincenzi, M., Sullivan, M., Möller, A., et al. 2023, MNRAS, 518, 1106
- Virtanen, P., Gommers, R., Oliphant, T. E., et al. 2020, Nature Methods, 17, 261